Andrzej Kubit
Wojciech Jurczak
Tomasz Trzepiecinski ✉
Koen Faes

https://doi.org/10.21278/TOF.44304
ISSN 1333-1124
eISSN 1849-1391

EXPERIMENTAL AND NUMERICAL INVESTIGATION OF IMPACT RESISTANCE OF RIVETED AND RFSSW STRINGER-STIFFENED PANELS IN BLUNT IMPACT TESTS

Summary

Aluminium alloy sheets have come into widespread use in the design of stringer-stiffened aerospace structures. This paper evaluates experimentally and numerically the response of stringer-stiffened Alclad 7075-T6 aluminium alloy panels subjected to impact loading. The aim of the study was to compare the impact resistance of riveted structures with the structures with the impact resistance of structures welded using the refill friction stir spot welding (RFSSW) process, which is a relatively new technique now used to create joints in aircraft structures. The experimental tests were carried out using a drop-weight type impact testing machine. Finite element modelling of stringer-stiffened panels under impact loading was carried out by using the nonlinear finite element-based MSC.Marc + Mentat program. The results of the numerical computations were validated against the experimental data. Studies were also made of the resistance of the joints to failure, the springback response and the stiffness of joints in the conditions of the dynamic impact test.

Key words: *blunt impact test; FEM, impact resistance; RFSSW; stiffened panel*

1. Introduction

Both composite and aluminium-based panels in aircraft can be damaged in high-speed impacts arising from chance events. Essentially, such events can be divided into two groups. The first group includes collisions of an aircraft with hailstones [1, 2] or birds [3, 4], while the second group includes impacts with tyre debris [5]. Hailstone impact on aircraft structures is a transient process, characterised by a high strain rate and high loading amplitude [6]. The impact of a bird or hailstone on an aircraft may cause damage to the aircraft fuselage or wing skins and is extremely dangerous for the safety of the aircraft. Such damage to the aircraft structure is usually associated with high impact speed and a relatively low mass of the object. However, most damage to aircraft structures due to random impacts with foreign bodies in civilian airplanes primarily takes place during ground handling [7]. Accidental impacts occur during loading or unloading and this is the most common cause of damage to structural elements of aircraft [7].

Ground-based damage caused by dynamic impacts is characterised by a relatively low speed of interaction as well as a significant mass of impacting objects. The authors of studies [8-10] define the speed range for low-speed collisions in the range of 1-10 m/s. However, in practice, the ground-based impact speed is up to about 2 m/s [3]. When conducting an experimental study or modelling the phenomena occurring in the events considered here, these phenomena are considered as quasi-static [3, 11]. In low-velocity impacts, the contact of the object with the structure is long enough for the whole structure to transfer the dynamic load, similarly to static load conditions [12, 13]. For impact tests in the low-speed range Charpy, Izod and drop-weight type impact testing machines are commonly used [8]. In the case of impact tests on aircraft structures using the aforementioned methods, the drop-weight type impact test captures the conditions of real random events related to the dynamic structure load most accurately [12, 14].

Most previous investigations focused on the experimental and numerical analysis of low-velocity impact on composite structures. Kim et al. [2] projected spherically shaped ice hailstones onto composite panels to determine the damage resistance of thin-walled composite structures to ice impact. Composite panel impact experiments show a linear relationship between the kinetic energy at which failure initiates and the thickness of the panel. Jackson and Poe [15] used dynamic analyses to define ranges of impact parameters where quasi-static analyses are valid. They found that for large mass impacts of moderately thick (3.5 to 7 mm) laminates, the maximum extent of delamination damage increased with increasing impact force and decreasing specimen thickness. Kim and Kerward [1] modelled hail ice impacts and predicted the initiation of impact damage in composite structures to measure both the impact energy at which damage initiates and the elastic response of a composite panel resulting from the impact. The high velocity impact response of aluminium alloy-based fibre metal laminates was investigated by Villanueva and Cantwell [16]. High velocity impact tests performed on sandwich structures resulted in a number of different failure modes. Coles et al. [17] conducted experiments on ice and steel projectile impact on carbon/epoxy composite flat plates to observe the damage and fracture differences on the front and the rear surface. The experiments have shown that, depending on the depth of indentation, fragmenting projectiles destroyed on impact resulted in a more distributed loading leading to major front surface damage.

Steel stiffened panels have been thoroughly investigated by experimental testing, analytical modelling and finite element-based techniques. Multi-stiffened aluminium alloy panels are used in a wide range of aircraft applications due to their good strength-to-weight ratio. The investigations of stringer-stiffened aluminium alloy panels mainly address their buckling resistance [18]. Morin et al. [19] tested stiffened 6062-T6 aluminium alloy panels subjected to low-velocity impact loading. It was found that failure in the stiffened panel was initiated by a ductile fracture process, while propagation seemed to be dominated by shear fracture. The results of Song et al. [20] show that 2024 aluminium alloy stringer-stiffened curved panel damage from ice sphere impacts is a stress wave dominated dynamic response and the initial delamination of the panel always occurs at the skin-stringer interface.

Mines et al. [21] investigated the dynamic response of aluminium sheets to rubber projectiles taken from an aircraft tyre taxiway. The impact velocities ranged between 75 and 135 m/s. The response of 5754 H111 aluminium alloy plates to rubber ball impacts at an impact velocity of 130 m/s was experimentally studied by Guégan et al. [5]. These measurements were used to evaluate the maximum strain induced in the sheet metal and to check if the sheet material is plastically deformed or not. Chen et al. [11] conducted quasi-static indentation and dynamic transverse impact experiments on stringer-reinforced composite panels using a D-shaped rubber bumper. It was concluded that accidental impacts happening under very slow loading rates can produce less detectable damage and may be located away from the impact site.

The results of investigations of composite structures under impact conditions are widely presented in the literature. However, the high-impact testing of aluminium alloy-based stringer-stiffened structures is limited. Although the aluminium alloy-based structures offer excellent in-plane performance, they are susceptible to failure when loaded out-of-plane. This paper evaluates experimentally and numerically the response of stringer-stiffened aluminium alloy panels subjected to impact loading. The aim of the study was to compare the impact resistance of riveted structures with the structures with the impact resistance of structures welded using the refill friction stir spot welding (RFSSW) process, which is a relatively new technique now used to create joints in aircraft structures [22]. The experimental tests were carried out using a drop-weight type impact testing machine. Numerical simulations of the impact tests were conducted by using the nonlinear finite element-based MSC.Marc + Mentat program. The resistance of the joints to failure and joint stiffness were studied in the conditions of the dynamic impact test.

2. Experimental methods

2.1 Material

The material of both stringer and plate was Alclad 7075-T6 precipitation-hardened aluminium alloy delivered by Trentwood Works (Spokane, WA, USA). Alclad 7075-T6 aluminium alloy cannot be welded by resistance welding. The thickness of the plate was 0.8 mm and the thickness of the S-shaped stringer was 1.6 mm. The mechanical properties of the 7075-T6 aluminium alloy determined in tensile tests are shown in Table 1. The average values of the basic mechanical properties were determined based on three measurements. The elemental composition of the 7075-T6 aluminium alloy (Table 2) was investigated by using an energy dispersive X-ray (EDX) spectrometer. EDX spectra were collected at 30 (kV) on a Quanta 3D 200i scanning electron microscope at a magnification of 300x.

Table 1 Mechanical properties of 7075-T6 aluminium alloy

Ultimate tensile stress R_m / (MPa)	Yield stress $R_{p0.2}$ / (MPa)	Elongation A_5 / (%)	Hardness HB
530	463	8	160

Table 2 Chemical composition of 7075-T6 aluminium alloy (wt. %)

Zn	Mg	Cu	Cr	Mn	Fe	Si	Ti	Al
5.60	2.61	1.35	0.26	0.06	0.10	-	0.05	remainder

2.2 Fabrication of stringer-stiffened panels

Samples for the impact test were prepared in the form of stringer-stiffened specimens (Fig. 1). Two types of connection (welded and riveted) in the overlapping configuration were used to join the stringer to the plate. Welded connections were made on a refill friction stir spot welder RPS100 by Harms & Wende GmbH & Co KG (Hamburg, Germany) at the Belgian Welding Institute (Zwijnaarde-Gent, Belgium). The RFSSW process can be briefly divided into three main stages (Fig. 2): touchdown, plunging and refilling, which were described in detail in a recent paper by the authors [22] and in the literature [23].

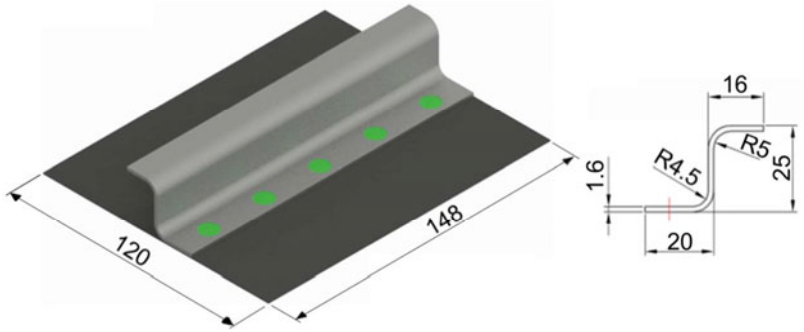

Fig. 1 Stringer-stiffened specimen (dimensions in mm)

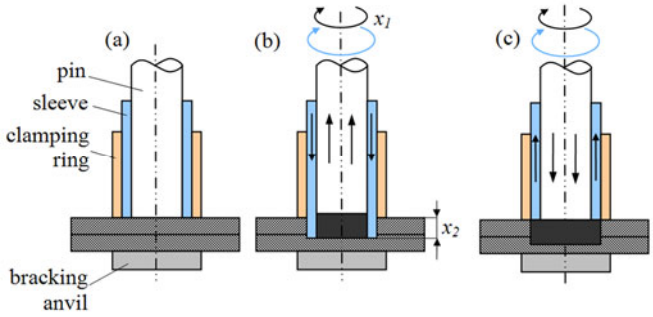

Fig. 2 Stages of the RFSSW process: (a) contact, (b) plunge and (c) refill

The parameters of the welding process are as follows: tool rotational speed v = 2000 rpm, tool plunge depth g = 1.8 mm, plunge time t_p = 2 s, dwell time t_d = 2 s, retraction time t_r = 2 s. The values of the parameters selected assured the most favourable joint quality in terms of the highest static strength and quality of the weld structure (the minimum number of structural discontinuities and of structural notches. In the case of the riveted configuration, the rivets were made of PA24 aluminium alloy which, according to the EN1301-2 standard, is the equivalent of the 2117 aluminium alloy. The diameter of the rivets was 3 mm. The rivets were compressed by using standard riveting equipment. The spacing between the joint depends on the diameter of the connector. The average rivet pitch in aircraft structures ranges from 4 to 8 rivet diameters. Rivet spacing on the parts that were subjected to bending moments is closer to the minimum spacing needed to prevent buckling of the skin [24]. In the case of riveted joints the typical pitch used in aircraft skin structures of p = 23.5 (Fig. 3a) mm was assumed. In the case of welded joints two spacings were considered. The diameter of the weld was three times greater than the rivet diameters. So, in the first configuration, according to the principle of the same distance between joint edges, a spacing of welds of p = 29.5 mm was used (Fig. 3b). Due to the larger area of the weld in relation to the rivet diameter, RFSS-welded samples with a spacing 50% larger (p = 44.25 mm) were also tested.

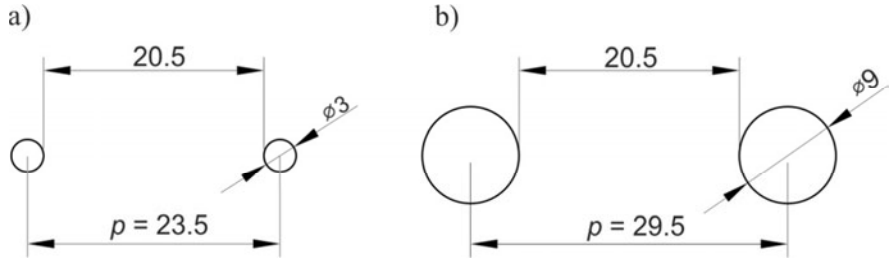

Fig. 3 Spacings between connectors in (a) riveted (p = 23.5 mm) and (b) welded (p = 29.5 mm) configurations (dimensions in mm)

2.3 Drop-weight impact test

Drop tests were conducted utilising a drop-weight type impact machine (Fig. 4) and a panel test fixture (Fig. 5). Impact was attained by dropping a 27-kg weight hammer and an 8.81-kg weight bumper from a height of 0.25 m. The impact bumper was positioned to collide in the centre of the stiffened panel. The outer radius of the curvature of the bumper was approximately 20 mm.

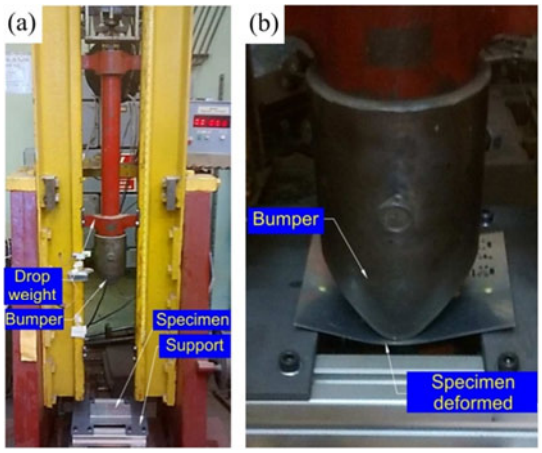

Fig. 4 Drop-weight blunt impact machine (a) and the deformed specimen (b)

The spot joints were in a one-row configuration. The aim of the dynamic load was permanent deflection of the joint in a direction transverse to the line of connectors. So, the joints were subjected to dynamic shear loading. In the dynamic load test, the geometrical quantities characterising the amount of elastic and plastic deformation of the specimens were measured. The load configuration analysed is a typical three-point bending, hence the values of the sample deflection were measured. The plastic deflection was determined after the impact test, whereas the elastic deflection was recorded by placing a modelling paste under the sample (Fig. 6).

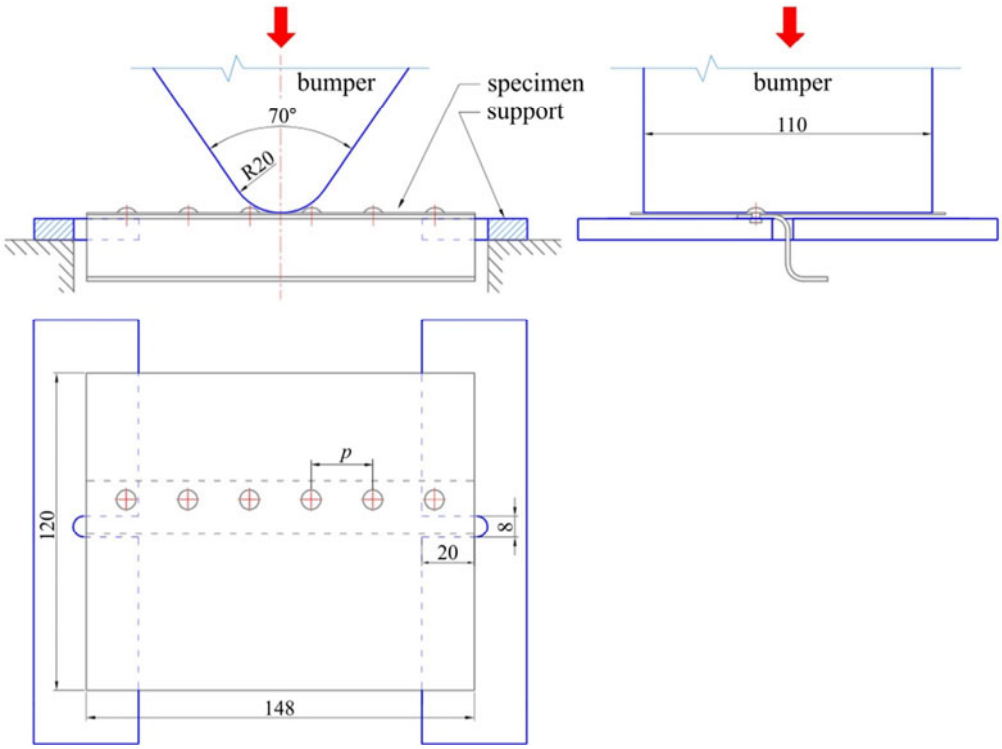

Fig. 5 Dimensions of the specimen and configuration of the drop-weight test fixture (dimensions in mm)

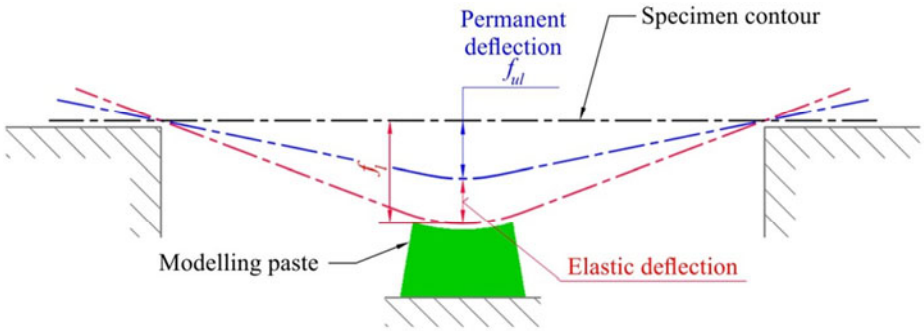

Fig. 6 Method of measurement of the elastic response of the stringer-stiffened panel after unloading

3. Numerical modelling

The numerical modelling of the panel deformation process was carried out in the finite element-based MSC.Marc + Mentat program for the analysis of physical models that takes into account geometric and material non-linearities. A quasi-static technique was used to analyse the results of the blunt impact test. The geometric model of the problem corresponds to the real dimensions of the study object (Fig. 7). Figure 7 presents initial mutual positions of the panel and the tools. The velocity of the bumper impacts on the panel corresponded to the experimental conditions. As the supports and the bumper were considered to be rigid, no deformation was assumed in these parts during the forming process. The displacements of the supports were fixed. The boundary conditions applied to the bumper allow displacement in the normal direction to the specimen surface. The bumper impact on the stringer-stiffened structure at velocity corresponded with the experiments (v = 2.42 m·s^{-1}). The analysed time was set to 0.008 s.

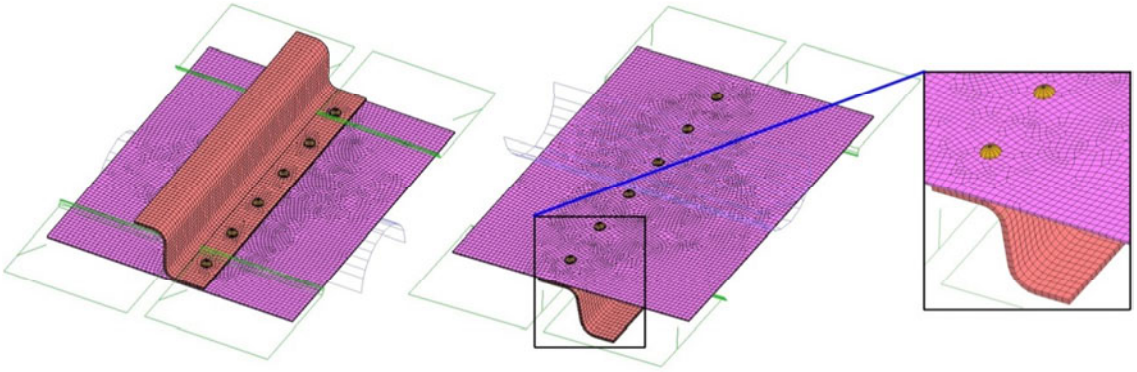

Fig. 7 Numerical model of the blunt impact test (riveted stringer-stiffened structure)

The blank was modelled with a three-dimensional, eight-node, isoparametric HEX8 element (arbitrarily distorted brick) [25]. The stiffness of this element is formed using an eight-point Gaussian integration. The assumed strain formulation is used to improve the bending behaviour of the elements. This increases the stiffness assembly costs per element, but improves the accuracy [25].

In the numerical modelling, both the riveted and the welded specimens were considered. In the case of the riveted structure, the real 3D geometry of the rivets was assumed. In the riveted variant of the panel, the sheet and stringer model was composed of 21,706 elements, while the rivets consisted of 4,248 linear elements, resulting in a total number of 25,954 elements. The total number of finite elements of the welded variants with a spacing of p = 29.5 mm and p = 44.25 mm was equal to 18,354 and 18,480 elements, respectively.

When generating a 3D mesh, the rule should be applied so that finite elements have the most regular shape (the ratio of the longest side to the shortest side should be close to one). The use of elements one of whose dimensions is much larger than the others generates errors related to the approximation of the searched values between nodes during calculations.

Welded joints were modelled using the so-called discrete multipoint connectors (MPCs). Discrete CWELD patch-to-patch connections were defined by specifying the location of lines connecting two or more surfaces (Fig. 8) [25]. The discrete connector locations are independent of the location of nodes in the element mesh and the density of the finite element mesh.

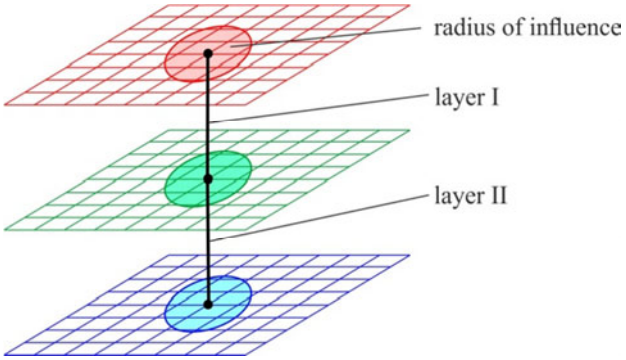

Fig. 8 Two-layer patch-to-patch connector configuration

The material model of the sheet and stringer is treated as elastic-plastic with nonlinear material behaviour as described by the von Mises yield criterion with the strain hardening effect. For the ideal case of isotropic materials, the von Mises yield condition is expressed as:

$$\overline{\sigma}^2=\frac{1}{2}\left[(\sigma_{11}-\sigma_{22})^2+(\sigma_{22}-\sigma_{33})^2+(\sigma_{33}-\sigma_{11})^2+3(\sigma_{12}^2+\sigma_{23}^2+\sigma_{31}^2)\right], \tag{1}$$

where $\overline{\sigma}$ is the equivalent stress, and indices *1*, *2*, *3* represent the rolling, transverse and normal direction to the sheet surface.

The isotropic hardening behaviour implemented in the FEM model uses the Hollomon power-type law expressed as:

$$\sigma_p=K\cdot\varepsilon^n \ , \tag{2}$$

where σ_p is the yield stress, ε is the plastic strain, K is the material constant and n the strain-hardening exponent.

The parameters in the Hollomon Eq. (2) were fitted on the stress-strain curve of the tensile test. The elastic behaviour is specified in numerical simulations by the value of Young's modulus, E = 71,700 MPa, and Poisson's ratio v = 0.33. The material density is set at ρ = 2,810 kg·m^{-3}. The material model of the rivets (PA24) is considered as elastic-plastic with the following values of the parameters: yield stress σ_p = 202 MPa, Young's modulus E = 71,000 MPa, Poisson's ratio v = 0.33, density ρ = 2750 kg·m^{-3}.

The contact between the assumed rigid bodies (the supports and the bumper) and the deforming workpiece as well as the contact between the base plate and the stringer were defined by specifying a friction coefficient of 0.1.

4. Results and discussion

The bumper was dropped from a height of 250 mm. This corresponds to an impact energy of 87.8 J. The impact velocity at the moment of collision of the bumper with the stringer-stiffened structure was equal to v = 2.42 m·s^{-1}. The amount of the panel springback was then evaluated as [26]:

$$K_s = \frac{f_{ul}}{f_l}, \tag{3}$$

where: f_{ul} is the deflection of the panel under unloading, f_l is the maximum depth of panel deflection (Fig. 5).

Both welded panels considered were stiffer than the riveted panel (Fig. 9). The panel consists of a stringer welded to the plate with a spacing of welds of p = 29.5 mm. The difference in the maximum depth of the panel deflection between the riveted structure and the RFSS-welded structure is about 4.6 mm (28%). This situation is influenced by various factors, including the lower stiffness of the riveted structure caused by the holes in the sheet and the stringer. Furthermore, the total area of the joint is higher in the case of the welded variants (the diameter of the rivet is 3 mm, the diameter of the welds is 9 mm). The panel welded with a spacing between welds of p = 44.25 mm exhibits the greatest amount of springback (Fig. 9). Decreasing the spacing between the welds to p = 29.5 mm led to a decrease in the value of the springback coefficient. In this case, due to the weld being located along the line of symmetry of the panel (Fig. 10b), the impact energy is concentrated along the lateral of the S-shaped stringer. The panel welded with a spacing between the welds of p = 44.25 mm exhibits the most deflection of the plate edges in the direction of impact (Fig. 10c). The verification of individual joints showed that the joints were never damaged by shearing, i.e. all of them remained coherent after the dynamic impact.

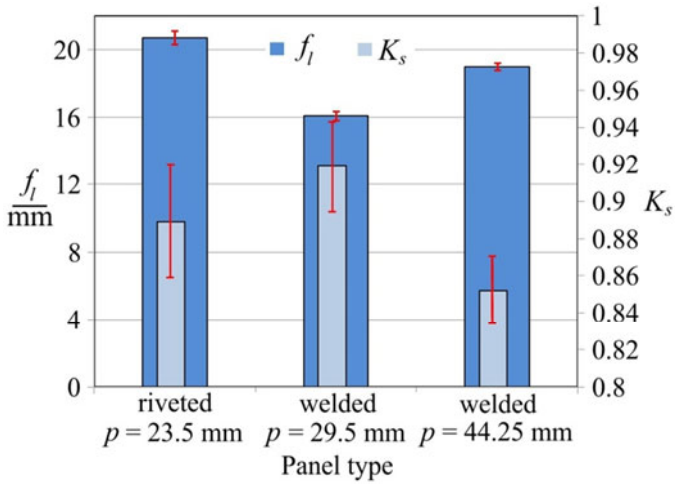

Fig. 9 Effect of panel type on the deflection of the panel under loading f_l and springback coefficient K_s

a)

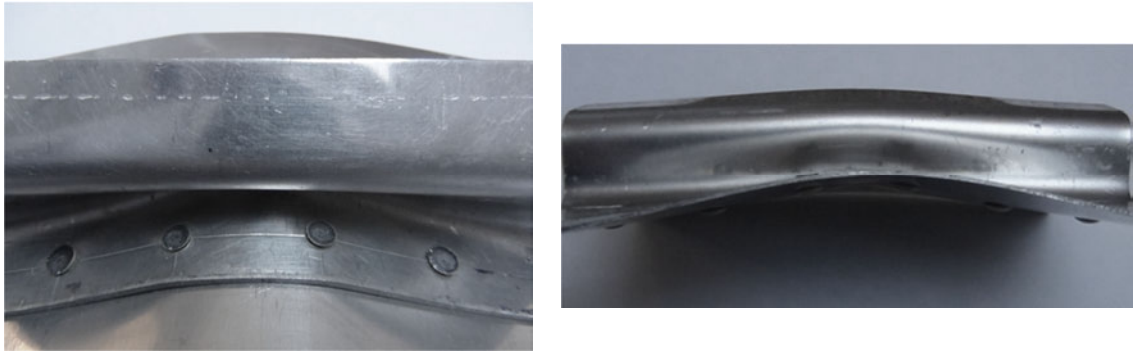

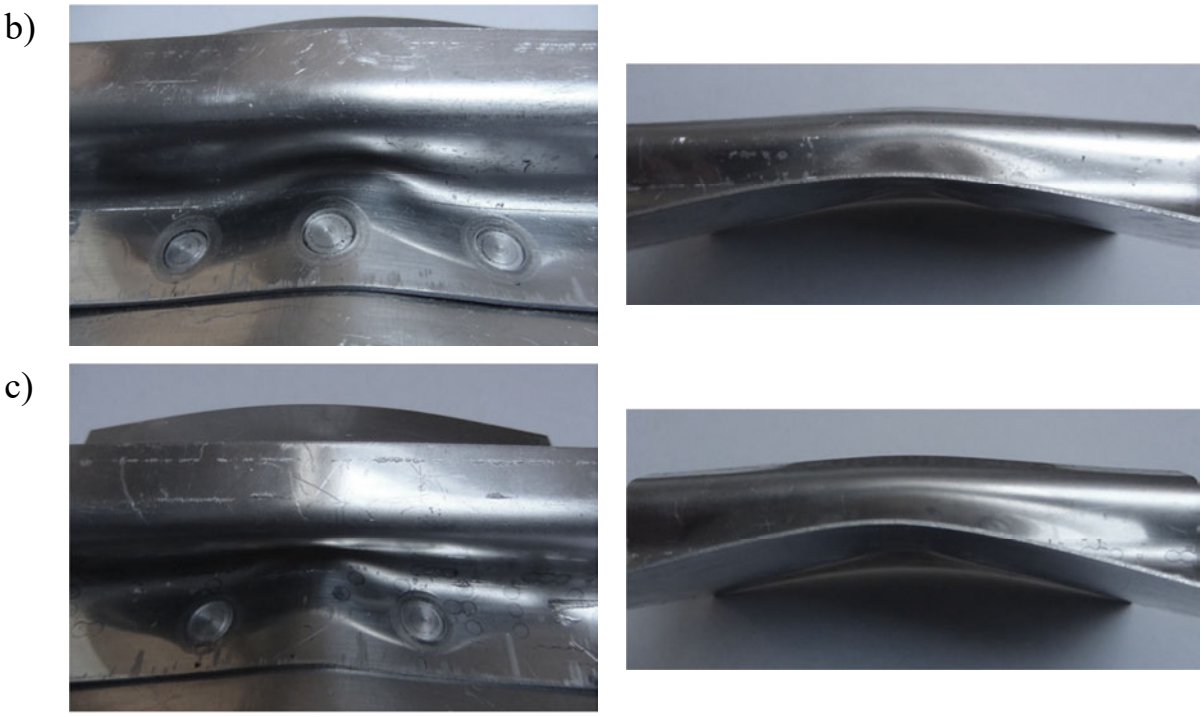

Fig. 10 Specimens after impact tests: (a) riveted panel with spacing between rivets of 23.5 mm, (b) welded panel with spacing between welds of 29.5 mm, (c) welded panel with spacing between welds of 44.25 mm

Fig. 11 shows the variation in the force of the bumper F_B during the collision with the panel. Due to the lower stiffness of the riveted panel, this panel lost its stability the most rapidly. This was manifested by reaching the maximum force in the fastest time. After reaching the maximum force F_B, the experimentally confirmed localisation of the deformation of the stiffener was observed in the form of a depression in the middle area of the specimen. Further deflection of the panel takes place with decreasing F_B force The highest stiffness was observed for the welded panel with a spacing between the welds of p = 29.5 mm. The values of the maximum equivalent von Mises stress in the welded panels in response to the largest movement of the bumper are similar (Fig. 12b, c). The increased stiffness of the welded panel with p = 29.5 mm in comparison with the welded panel with a spacing p = 44.25 mm resulted in the values of stresses observed at different deflection values.

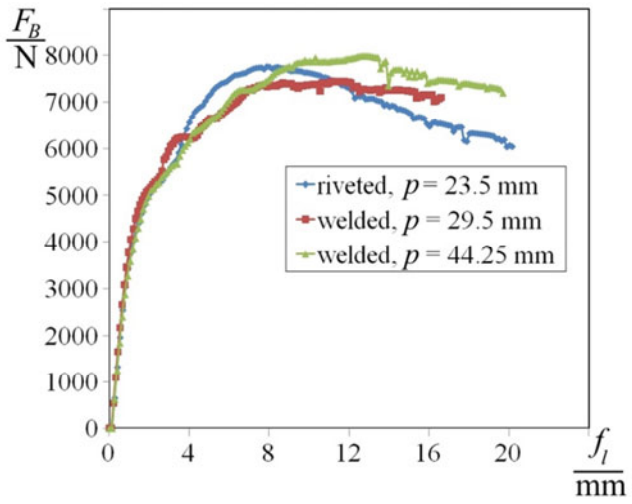

Fig. 11 Numerically predicted bumper force F_B *vs*. panel deflection f

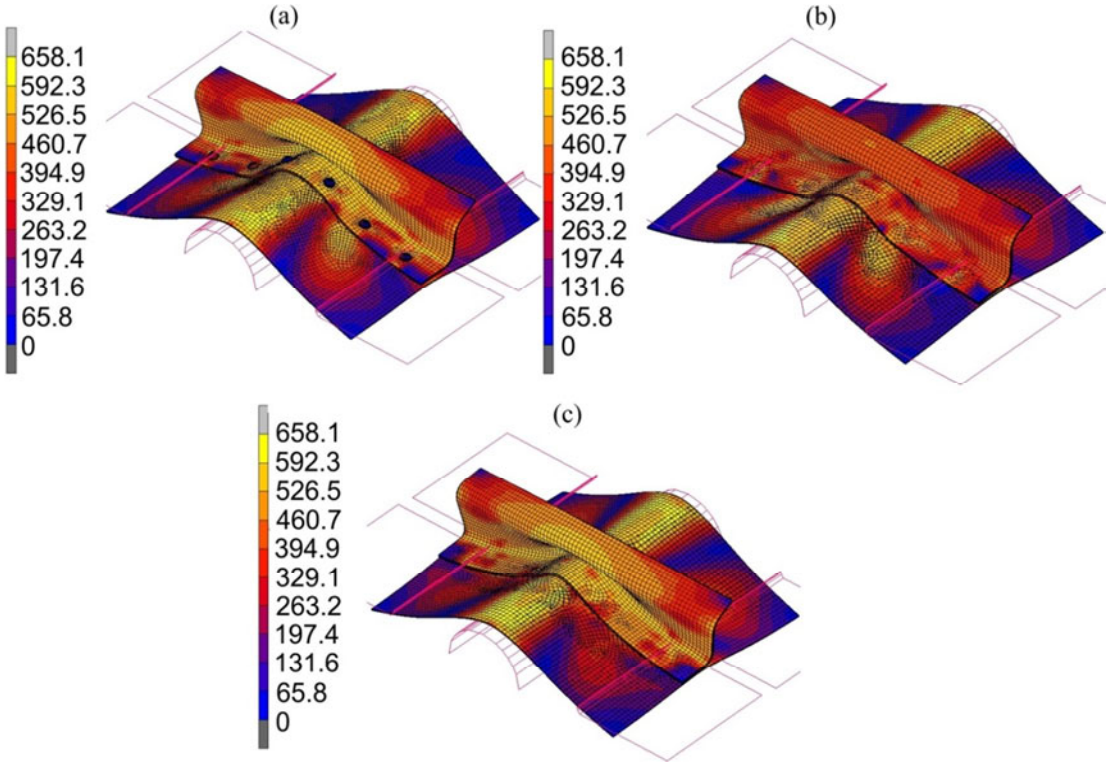

Fig. 12 Distribution of equivalent von Mises stress (MPa) at maximum panel deflection: (a) riveted panel (p = 23.5 mm), (b) welded panel (p = 29.5 mm), (c) welded panel (p = 44.25 mm)

The highest value of the equivalent stress in the riveted panel (Fig. 12a) was about 4% higher than in the welded panels. The increased stress values were mainly observed in the area of the rivets. In all of the analyzed panel types, symmetrical longitudinal bending was observed (Fig. 13). This is a result of a significant reduction in the height of the S-shaped stringer in the location where the bumper impacts the panel. The numerically predicted distortion of the S-shaped stringer corresponded well with the experiments in all the cases analysed.

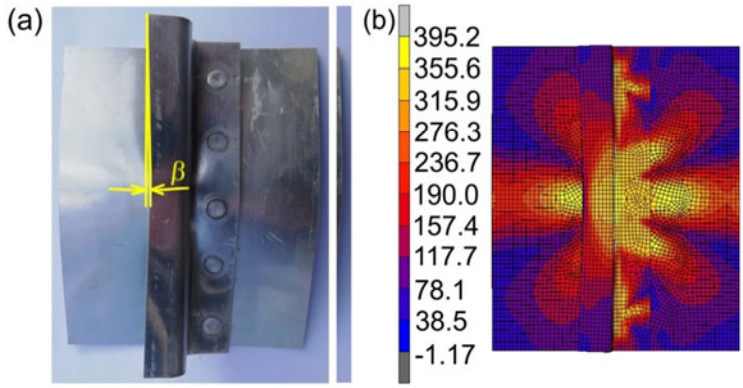

Fig. 13 Front view of the welded panel (p = 29.5 mm): (a) specimen, (b) distribution of equivalent von Mises stress (MPa) in the numerical model of the specimen

5. Conclusions

The main conclusions drawn from the experimental and numerical analyses are as follows:

- the RFSSW joints exhibit a higher resistance to dynamic impact in comparison with riveted joints,
- the RFSSW joints in the configuration of the study panel have a greater stiffness than single-lap riveted joints,

- the stiffness of the welded joints increases with decreasing of the spacing between welds,
- decreasing the spacing between welds led to a decrease in the springback coefficient value due to local concentration of deformation in the middle part of the S-shaped stringer,
- the welded panels lost stability at a similar value of material effort, however, the deflection of the panel welded with a weld spacing p = 29.5 mm is 15% lower than the deflection of the panel welded with a weld spacing p = 44.25 mm,
- comparing all cases of panels analysed, the riveted panel lost stability at the lowest movement of the bumper.

REFERENCES

[1] Kim, H.; Kedward, K. T. Modeling Hail Ice Impacts and Predicting Impact Damage Initiation in Composite Structures. *American Institute of Aeronautics and Astronautics Journal* **2000**, 38(7),1278–1288. https://doi.org/10.2514/2.1099

[2] Kim, H.; Welch, D. A.; Kedward, K. T. Experimental Investigation of High Velocity Ice Impacts on Woven Carbon/Epoxy Composite Panels. *Composites Part A: Applied Science and Manufacturing* **2003**, 34(1), 25–41. https://doi.org/10.1016/S1359-835X(02)00258-0

[3] Defrancisci, G. K.; Chen, Z. M.; Kim, H. Blunt Impact Damage Formation in Frame and Stringer Stiffened Composite Panels. Proceedings of 18th International Conference On Composite Materials. 21th-26th August 2011 Jeju Island, South Korea, p. 1–6.

[4] Zbrowski A. The Safety of Aircraft in the Aspect of the Danger of Collision with Birds. *Journal of Machine Construction and Maintenance* **2012**, 2, 215–227.

[5] Guégan, P.; Othman, R.; LeBreton, D.; Pasco, F.; Swiergiel, N.; Thevenet, P. Experimental Investigation of Rubber Ball Impacts on Aluminium Plates. *International Journal of Crashworthiness* **2010**, 15 (4), 391–399. https://doi.org/10.1080/13588260903504044

[6] Tang, Z.; Hang, C.; Suo, T.; Wang, Y.; Dai, L.; Zhang, Y.; Li, Y. Numerical and experimental investigation on hail impact on composite panels. *International Journal of Impact Engineering* **2017**, 105, 102–108. https://doi.org/10.1016/j.ijimpeng.2016.05.016

[7] International Air Transportation Association. Ground Damage Prevention Programme Targets 10% Cost Reduction. *Industry Times* **2015**, Article 4.

[8] Safri, S. N. A.; Sultan, M. T. H.; Yidris, N.; Mustapha, F. Low Velocity and High Velocity Impact Test on Composite Materials – A review. *The International Journal of Engineering and Science* **2014**, 3(9), 50–60.

[9] Shivakumar, K. N.; Elber, W.; Illg, W. Prediction of Low Velocity Impact Damage in Thin Circular Laminates. *American Institute of Aeronautics and Astronautics Journal* **1985**, 23(3), 442–449. https://doi.org/10.2514/3.8933

[10] Niewerth, D.; Stefaniak, D.; Hühne, C. The Response of Hybrid Composite Structures to Low-Velocity Impact. Proceedings of 16th International Conference on Experimental Mechanics, 7th-11th July 2014, Cambridge, UK, p. 1–2.

[11] Chen, Z. M.; Kim, H.; Defrancisci, G. K. Experimental and Modeling Investigation of Blunt Impact to Stringer-Reinforced Composite Panels. Proceedings of 28th Annual Technical Conference of the American Society for Composites. 9th-11th September 2013, Pennsylvania, USA, p. 1848–1867.

[12] Cantwell, W. J.; Morton, J. The Impact Resistance of Composite Materials - A Review, *Composites* **1991** 22 (5), 347–362. https://doi.org/10.1016/0010-4361(91)90549-V

[13] Richardson, M. O. W.; Wisheart, M. J. Review of Low-Velocity Impact Properties of Composite Materials, *Composites Part A: Applied Science and Manufacturing* 1996, 27(12), 1123–1131. https://doi.org/10.1016/1359-835X(96)00074-7

[14] Mathivanan, N. R.; Jerald, J. Experimental Investigation of Low-Velocity Impact Characteristics of Woven Glass Fiber Epoxy Matrix Composite Laminates of EP3 Grade, *Materials and Design* **2010**, 31(9), 4553–4560. https://doi.org/10.1016/j.matdes.2010.03.051

[15] Jackson, W.; Poe, C. The Use of Impact Force as a Scale Parameter for the Impact Response of Composite Laminates, *Journal of Composites, Technology and Research* **1993**, 15(4), 282–289. https://doi.org/10.1520/CTR10380J

[16] Villanueva, R. G.; Cantwell, W. J. The High Velocity Impact Response of Composite and FML-Reinforced Sandwich Structures. Composites Science and Technology **2004**, 64(1), 35–54. https://doi.org/10.1016/S0266-3538(03)00197-0

[17] Coles, L. A.; Roy, A,; Voronov, L.; Semeyonov, S.; Nikhamkin, M.; Silberschmidt, V. V. Dynamic Fracture in Carbon-Fibre Composites: Effect of Steel and Ice Projectiles. Procedia Structural Integrity **2016**, 2, 366–372. https://doi.org/10.1016/j.prostr.2016.06.047

[18] Teixeira-Dias, M. F.; F, Valente, R. A. F. Numerical Simulation of Aluminium Stiffened Panels Subjected to Axial Compression: Sensitivity Analyses to Initial Geometrical Imperfection Sand Material Properties. *Thin-Walled Structures* **2013**, 62, 65–74. https://doi.org/10.1016/j.tws.2012.07.024

[19] Morin, D.; Kaarstad, B. L.; Skajaa, B.; Hopperstad, O. S.; Langseth, M. Testing and Modelling of Stiffened Aluminium Panels Subjected to Quasi-Static and Low-Velocity Impact Loading. *International Journal of Impact Engineering* **2017**, 110, 97–111. https://doi.org/doi.org/10.1016/j.ijimpeng.2017.03.002

[20] Song, Z.; Le, J.; Whisler, D.; Kim, H. Skin-Stringer Interface Failure Investigation of Stringer-Stiffened Curved Composite Panels Under Hail Ice Impact. *International Journal of Impact Engineering* **2018**, 122, 439–450. https://doi.org/10.1016/j.ijimpeng.2018.09.014

[21] Mines, R. A. W.; McKown, S.; Birch, R. S. Impact of Aircraft Rubber Tyre Fragments on Aluminium Alloy Plates: I – Experimental. *International Journal of Impact Engineering* **2007**, 34(4), 627–646. https://doi.org/10.1016/j.ijimpeng.2006.02.005

[22] Kubit, A.; Bucior, M.; Wydrzyński, D.; Trzepiecinski, T.; Pytel, M. Failure Mechanisms of Refill Friction Stir Spot Welded 7075-T6 Aluminium Alloy Single-lap Joints. *International Journal of Advanced Manufacturing Technology* **2018**, 94(9-12), 4479–4491. https://doi.org/10.1007/s00170-017-1176-2

[23] Schilling C, dos Santos J. Verfahren und Vorrichtung zum verbinden von wenigstens zwei aneinanderliegenden Werkstücken nach der Methode des Reibrührschweißens. Patent DE 199 55 737 B4 2005.11.10.

[24] http://www.flight-mechanic.com/structural-fasteners-solid-shank-rivets-installation-of-rivets/

[25] Marc 2010, Volume A: Theory and User Information. MSC.Software Corporation, Santa Ana, 2010.

[26] Trzepiecinski, T.; Lemu, H. G. Effect of Computational Parameters on Springback Prediction by Numerical Simulation. *Metals*, **2017**, 7(9), article no. 380. https://doi.org/10.3390/met7090380

Submitted: 05.4.2019

Accepted: 17.3.2020

Andrzej Kubit
Department of Manufacturing and Production Engineering
Rzeszow University of Technology
Al. Powst. Warszawy 8, 35-959 Rzeszow, Poland
E-mail: akubit@prz.edu.pl

Wojciech Jurczak
Polish Naval Academy
Faculty of Mechanical and Electrical Engineering
ul. Śmidowicza 69, 81-127 Gdynia, Poland
E-mail: w.jurczak@amw.gdynia.pl

Tomasz Trzepiecinski
(corresponding author)
Department of Materials Forming and Processing
Al. Powst. Warszawy 8, 35-959 Rzeszow, Poland
E-mail: tomtrz@prz.edu.pl

Koen Faes
Belgian Welding Institute
Technologiepark-Zwijnaarde 935, 9052 Gent, Belgium
E-mail: Koen.Faes@bil-ibs.be